

Ignition Characteristics of Diesel and Canola Biodiesel Sprays in the Low-Temperature Combustion Regime

Casey M. Allen, Elisa Toulson, David L. S. Hung, Harold Schock, Dennis Miller, and Tonghun Lee*

Department of Mechanical Engineering, Michigan State University, East Lansing, Michigan 48824, United States

ABSTRACT: The objective of this work is to investigate the spray ignition characteristics of diesel and canola-derived biodiesel in a rapid compression machine at the low temperatures (676–816 K) and reduced oxygen concentrations (12 and 18%) that are used in low-temperature combustion strategies of advanced diesel engines. A method for testing ignition delay times and apparent heat release rates at a series of temperatures is developed and characterized, whereby a given temperature is attained prior to the fuel spray by altering the charge cooling time after the end of compression. A single-zone heat release model is formulated and used with the experimental pressure data to calculate two unique ignition delay periods. For diesel, the total ignition delays measured with this approach are found to correlate very well with diesel ignition delay data published in the literature. When the first ignition delay period is compared, which approximates the initial time of heat release after the start of injection, it is noted that biodiesel ignites marginally faster (<1 ms) than diesel. However, the total ignition delay period, which measures the time to reach the maximum heat release rate after the start of injection, shows that canola-derived biodiesel ignites 23% faster than diesel under the tested conditions. The total ignition delay data also indicates decreased temperature sensitivity at increasing test temperature, which may be evidence of negative temperature coefficient behavior. The decrease in temperature sensitivity occurs at a lower temperature for diesel (~740 K) than for canola-derived biodiesel (~770 K). The sensitivities of the ignition delay times and the apparent heat release rates to changes in oxygen and fuel concentrations are also reported. It is noted that, when the maximum apparent heat release rates are normalized by the total ignition delay and on an input energy basis, the biodiesel and diesel fuels are remarkably similar for the tests using 12% oxygen but are distinguishable for tests using 18% oxygen at reaction zone temperatures in excess of 700 K.

1. INTRODUCTION

News outlets and scientific publications abound with evidence of a deteriorating environment and the risk of relying on foreign energy sources.^{1–3} A worldwide dependence upon fossil fuel energy underlies this problem and must be addressed by displacing fossil fuels with alternative fuels. The long-term successful replacement of fossil fuels will require new and novel approaches to energy generation. However, short-term solutions must be easily integrated with existing energy infrastructure, namely, combustion technology.

An important step to integrating new fuels into existing engines is the ability to model the engine operation using the physical properties and chemical ignition properties of the fuels. The mechanism, which can be coupled with advanced physical models that describe spray breakup, droplet evaporation, and turbulent mixing within the engine. Together, these models comprise computational fluid dynamics (CFD) simulations, which are essential in the engineering process for the development of new engines. It is critical that these models be supplied with accurate kinetic data to achieve meaningful and reliable modeling results. However, for some fuels, kinetic data are limited, which is especially true for nonvolatile fuels, such as petroleum-based diesel (petrodiesel) and biodiesel. The lack of kinetic data for nonvolatile fuels is largely due to the extreme temperatures required to vaporize sufficient fuel quantities to form a premixed charge of fuel and oxidizer gases; these elevated temperatures lead to thermal decomposition of the fuel (i.e., fuel cracking).

Given the challenge of acquiring gas-phase kinetic data for diesel and biodiesel, other approaches must be pursued to supplement modeling efforts by developing a practical understanding of how the spray ignition properties of these fuels respond to changes in engine operating conditions. In this study, a rapid compression machine (RCM) equipped with a fuel injector is used to compare the spray ignition processes of canola-derived biodiesel (BD) and reference-grade #2 petroleum-based diesel (D2). The test conditions created in the RCM for this study are consistent with diesel engine conditions, and the ignition delay and heat release rate data describe the ignition behavior of these fuels under realistic engine conditions. Although the gas-phase kinetics are not decoupled from the evaporation process, it has long been recognized that molecular-level fuel properties that influence ignition also affect evaporation,^{4,5} and these data fully describe the evaporation and ignition behavior that may be seen in an engine. Furthermore, the chemical ignition and evaporation processes in these tests may be partially decoupled through heat-loss analysis, which makes the data more fundamental in nature by estimating the first appearance of heat release from the fuel as it ignites. A RCM is a useful device for measuring the ignition characteristics of a fuel spray because the test chamber achieves a constant volume prior to ignition and the elevated test temperatures are generated by compressing the test gas, which leaves the wall temperature

Received: April 7, 2011

Revised: June 12, 2011

Published: June 14, 2011

nearly unchanged. This is in contrast to constant-volume combustion bombs where electrically heated walls may influence the ignition process in combination with the changes in the gas temperature.

The objectives of this study are to develop a systematic approach for testing fuel spray autoignition in an RCM and to use the approach to study the ignition characteristics of canola-derived BD and D2 fuel sprays. The test conditions used to characterize the ignition behavior of these fuels are modeled after the thermal and oxidative conditions seen in low-temperature combustion (LTC) strategies of clean diesel technology. Low combustion temperature conditions (<1800 K) are sought in LTC to avoid NO_x formation that is associated with high combustion temperatures in conventional diesel combustion.⁶ Additionally, LTC modes commonly inject fuel early to allow for additional fuel and air mixing time, which helps to minimize soot formation during combustion. To prevent the fuel from igniting too early, a large amount of cooled exhaust gas recirculation (EGR) is used to prolong the ignition delay.⁷ The EGR reduces the available oxygen in the cylinder, and as such, the test conditions in this study use oxygen fractions of less than 21%. The results of this study will give insight into the autoignition processes of diesel and biodiesel after injection into low-temperature oxidizing atmospheres and will contribute to the modeling and development of advanced compression-ignition engines.

1.1. Background. Diesel ignition delays have been reported in many prior studies. These data are most commonly measured for fuel sprays in RCMs,^{8–10} combustion bombs,^{11–13} or motored engines.^{14–16} The earliest known investigation of diesel ignition delays was completed by Wolfer¹³ in a combustion bomb. In that work, an ignition delay correlation was proposed in Arrhenius-like form. The proposed ignition delay correlation included the total physical delay time (atomization, vaporization, and mixing) and the chemical delay time. Since then, many studies have appeared in the literature with measurements of diesel fuel ignition delay times and some with modified coefficients for the Arrhenius ignition delay correlation.^{9,14,17,18} Of particular relevance to this study are the correlations established using data measured in constant volume devices (i.e., RCMs or combustion bombs). The results from these studies will be scaled according to the coefficients proposed by the respective authors and compared to our experimental results in a subsequent section.

Measurement of diesel fuel ignition delays remains a research topic of interest today. New approaches are being applied to elucidate the gas-phase kinetics of the fuel. A recent study by Haylett et al.¹⁸ employed an aerosol shock tube, which uses the incident shock to vaporize the fuel before the reflected shock ignites the mixture. This is a new approach to investigating gas-phase ignition delays of nonvolatile fuels and enables the fuel to be tested under well-defined conditions. Additionally, the authors of this work have recently proposed a charge preparation method in the RCM, which will enable testing of fuels with volatility that is similar to that of diesel.

Numerous studies regarding the reactivity of biodiesel, its primary constituents, and proposed biodiesel surrogates have also been published.^{19–21} As previously noted, gas-phase ignition delay measurements for fatty acid alkyl esters are particularly difficult to obtain as the length of the fatty acid alkyl chain or alkyl ester chain grows. For example, creation of a stoichiometric mixture ($p_0 = 1$ bar and $X_{O_2} = 0.21$) of methyl decanoate (C₁₀ methyl ester) in air requires an initial temperature near $T_0 = 110$ °C. The use of initial temperatures in gross excess of this

Table 1. Canola Biodiesel and Petrodiesel Fuel Properties

property	canola biodiesel	petrodiesel
molecular formula (estimated)	C _{18.82} H _{34.96} O ₂	C ₁₄ H ₂₅
heat of combustion (LHV) (MJ/kg)	37.3 ³²	42.98 ²³
density at 15 °C (g/mL)	0.883 ³³	0.834 ²³
viscosity at 40 °C (mm ² /s)	4.34 ³³	2.56 ²³
surface tension (mN/m)	23.6 ³⁴	25.2 ³⁵
boiling range (°C)	338–366 ³⁶	161–371 ³⁷
cetane number	47.9–56 ²	47–49.8 ^{23,38}

leads to concerns regarding fuel cracking and seal degradation and, in general, has prohibited the investigation of a meaningful range of test conditions for the high-molecular-weight methyl esters in biodiesel. Studies in the literature regarding biodiesel combustion characteristics are frequently completed in engines where physical and chemical events are linked, and occur in a temporally varying volume.^{22–24} These studies also frequently focus on applied issues, such as emissions; however, there are exceptions. Vaughn et al.²⁵ reported ignition delay times of bioester fuel droplets in a heated, constant-volume tube furnace. In their study, single methyl ester fuel droplets were injected into the furnace and tracked with a high-speed camera until OH* chemiluminescence was recorded, indicating the onset of ignition. The authors suggest that methyl oleate may be used as a surrogate for biodiesel based on similar ignition delay times between methyl oleate and a blend of soy methyl esters. In a more recent publication by Marchese et al.,²⁶ the same tube furnace was used to compare the ignition delay times for methyl oleate and soy methyl ester blends under microgravity conditions by placing the furnace into a 1.1 s drop tower. Subjecting the fuel droplet to microgravity conditions enabled Marchese et al.²⁶ to make a more adequate comparison to a numerical model, which assumed a spherically symmetric droplet.

Publications by Knothe et al.^{27–29} employed an ignition quality tester for measuring derived cetane numbers (DCNs) of straight-chain and branched alkyl esters of biodiesel. The tests were intended to characterize DCN dependence upon the form of alkyl ester and alkyl chain functional groups found in biodiesel compounds. The results indicate that biodiesel properties, including DCN, can be improved by engineering the structure of the biodiesel constituents. For example, Knothe et al. indicate that branching in the alkyl ester is favorable for cold-flow properties but has minimal influence on the DCN of the fuel.²⁷

2. EXPERIMENTAL SECTION

2.1. Rapid Compression Machine and Test Protocol. A RCM has been used in this study to investigate the spray-ignition characteristics of canola-derived BD and petroleum-based D2. Both fuels are intended for use in compression-ignition engines, but each fuel has unique properties, as summarized in Table 1. The RCM, which appears in Figure 1, is pneumatically driven and hydraulically stopped. It uses the mechanical stroke of a piston to generate elevated temperatures and pressures for combustion under constant-volume conditions. A creviced piston based on the design by Mittal and Sung³⁰ is used to promote the formation of a homogeneous core gas region during compression. The primary design elements of the RCM have been described in a prior publication;³¹ however, modifications have been made to the RCM for this study to enable direct injection of the fuel into the test chamber. The fuel system consists of a multi-hole inward-opening fuel injector, which is

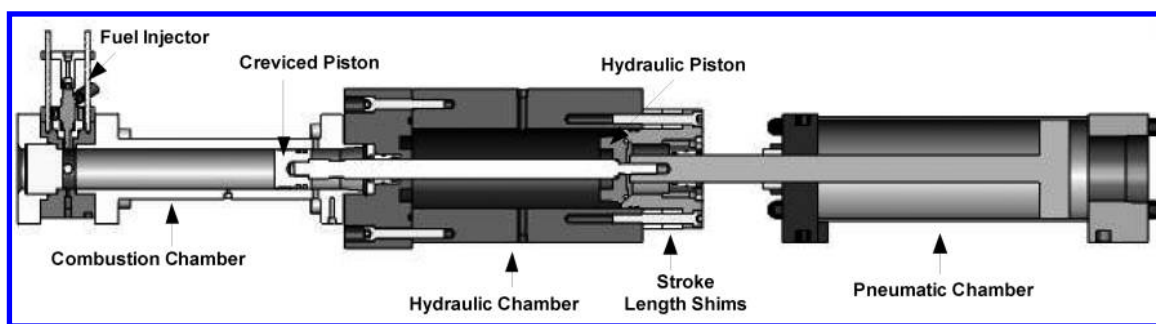


Figure 1. RCM schematics illustrating the primary components of the machine, including the mounting orientation for the fuel injector.

Table 2. Summary of Test Conditions for Experiments

all tests	compressed pressure, p_c (bar)	30			
	bulk equivalence ratio, φ	0.25			
	compression ratio, CR	12.7:1			
	fuel temperature, $T_{f,0}$ (K)	298			
	fuel pressure, p_f (bar)	100			
fuel injector	number of holes	7			
	hole diameter, d (μm)	200			
	discharge coefficient, C_D^a	0.33			
mixture	diluent ratio, $N_2/(N_2 + Ar)$	O_2 mole fraction, X_{O_2}	fuel mass injected, m_f (mg)	reaction zone temperature, T_{RZ} (K)	injection time ATDC, $t_{inj,ATDC}$ (ms)
mix 1	1.0	0.12	BD: 9.0–10.4 D2: 7.7–9.0	683–714	9.1–129.1
mix 2	1.0	0.18	BD: 13.1–15.4 D2: 11.4–13.3	676–708	3.6–100.3
mix 3	0.8	0.12	BD: 8.9–10.1 D2: 7.7–8.8	720–748	23.8–137.2
mix 4	0.8	0.18	BD: 13.0–14.9 D2: 11.3–12.9	711–741	10.7–86.9
mix 5	0.6	0.12	BD: 7.9–9.4 D2: 6.8–8.1	771–816	6.3–96.4
mix 6	0.6	0.18	BD: 12.2–14.3 D2: 10.6–12.4	751–791	6.9–89.6

^a Calculated using injector calibration data and eq 1 by Jung et al.⁴¹

fed liquid fuel from a hydraulic accumulator. The accumulator is used to pressurize the fuel line to 100 bar during testing. A single injector model is used for all tests, so that fuel effects are adequately compared without considering the effects of changing injector parameters. The general test approach involves compressing a mixture of oxygen and diluent gases and, subsequently, spraying a known quantity of fuel into the test chamber once the desired conditions are achieved. The timing and duration of the fuel spray is controlled by a LabView virtual instrument (VI). During compression, the VI monitors and records voltage data from a Kistler 6125B piezoelectric pressure transducer and charge amplifier setup. Once the pressure reaches a given threshold, a hardware trigger is activated, which the VI considers to be at time $t = 0$. The piston reaches top dead center (TDC) some time later (~ 8 ms). The exact time of piston arrival at TDC is accurately known from a calibration procedure performed for each unique test condition. Timing for the start of injection (SOI) may be set in the VI to take place anywhere after the trigger occurs, with resolution on the order of 10 μs . All tests

reported in this study set the SOI to occur at some time delay after TDC (ATDC).

The effect of the temperature on the ignition delay and heat release rate of BD and D2 fuel sprays has been studied at various temperatures, oxygen concentrations, and fuel concentrations, as described in Table 2. Tests were conducted at reaction zone temperatures of $676 \leq T_{RZ} \leq 816$ K using oxygen mole fractions of $X_{O_2} = 0.12$ and 0.18. All tests have been completed using a compressed pressure of $p_c = 30$ bar and a bulk equivalence ratio of $\varphi = 0.25$, which is calculated assuming that the fuel is fully vaporized and mixed with the oxygen and diluent gases. The bulk equivalence ratios have been calculated by assuming average formulas of $C_{18.82}H_{34.96}O_2$ for the canola BD and $C_{14}H_{25}$ for the D2. These estimations are consistent with other studies in the literature^{2,39,40} and enable the fuels to be tested at similar carbon concentrations. The equivalence ratios are calculated on an oxygen basis using the 12 and 18% oxygen fractions contained in the test mixtures. The RCM was configured with a compression ratio of 12.7:1. The compressed

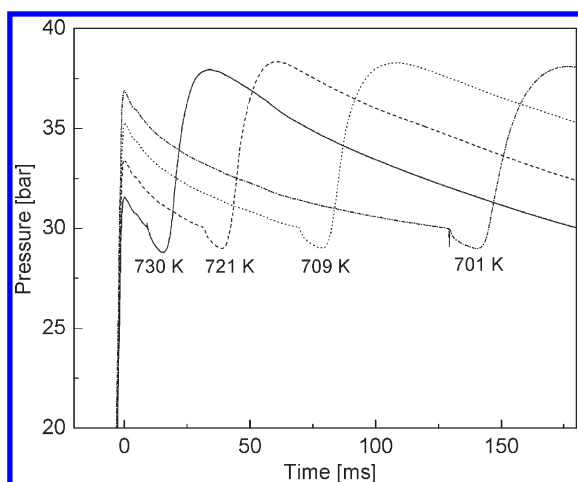


Figure 2. Sample set of reactive pressure history curves (canola BD, $X_{O_2} = 0.12$) that illustrate the injection timing approach that is used to generate the desired test temperatures. Each curve is marked with the calculated gas temperature at the time of injection.

temperatures have been adjusted by altering the composition of the diluent gas (nitrogen/argon ratio) and by changing the injection timing. As noted, all gas mixtures contained either 12 or 18% oxygen, while the diluent gases nitrogen and argon comprised the balance of the mixture. Argon accounted for 0, 20, and 40% of the diluent gas composition, with increases in the argon mole fraction bringing about a corresponding increase in compressed temperature. For each diluent gas composition used, an additional set of compressed temperatures were tested by allowing the gas mixture to cool for varying amounts of time after compression before commencing the fuel injection. This approach is illustrated in Figure 2, where tests for four different compressed temperatures are conducted using a single gas mixture and a single compression ratio. The temperatures describing each pressure curve in Figure 2 are adiabatic core temperatures and have been calculated using the effective volume approach described by Tanaka et al.⁴² and Mittal and Sung.³⁰ These core temperatures are considered valid up to the time of injection. The initial pressures for the tests are determined in advance to yield the desired compressed temperature when the cylinder pressure reaches 30 bar during cooling.

2.2. Assessment of the Test Approach. Many studies in the literature have been devoted to characterizing the adiabatic core region of gas that can be generated in RCMs.^{43–50} One focus of these studies has been to identify the spatial extent and temporal duration over which the core conditions prevail before degenerating because of convective and diffusive transport. A brief review of these studies is relevant because of the approach used in this study, where core conditions form the basis for characterizing the gas temperature up to 140 ms after the end of compression. It is important to know if the adiabatic core temperature calculations may be considered valid at such post-compression times where they serve as an input to estimate the temperature of the reactive charge after the fuel spray has evaporated. The review will be limited to studies that have employed a creviced piston, as in the RCM described in this paper. Creviced pistons are known to suppress vortex formation during compression and thereby improve the persistence and spatial extent of core conditions in the RCM.^{43,44,48} This is a critical feature in our study because it promotes the viability of core temperature calculations long after the end of compression.

The machining of a crevice around the periphery of a RCM piston crown was first proposed by Park and Keck.⁵¹ A preliminary comparison to a flat piston (i.e., no crevice) demonstrated that the crevice did reduce the rate of heat transfer to the test chamber walls and make the compression more isentropic in nature. However, no calculations or

measurements were presented to characterize the temperature or velocity fields in the core. Subsequent studies by Lee and Hochgreb⁴⁴ and Würmel and Simmie⁴⁹ were each concerned with crevice optimization for a particular RCM. CFD model results reported in each of these studies indicated that the extent of the core region is augmented significantly by the presence of a piston crevice. However, results were only presented for relatively short post-compression times (<30 ms). A more complete set of experimental and numerical results were reported by Mittal and Sung⁴⁸ in their study of post-compression temperature and velocity fields generated by creviced and flat pistons. Measurements using acetone planar laser-induced fluorescence (PLIF) sought to identify the time at which core gas temperatures were reduced because of mixing with the roll-up vortex. Tests indicated that temperature uniformity across the core is a function of the compressed pressure, p_c , and that the degree of uniformity may be greatly enhanced for tests at $p_c = 39.5$ bar relative to tests at $p_c = 11.95$ bar. For the tests at $p_c = 39.5$ bar, no core temperature inhomogeneity was observed at 114 ms post-compression, and even at 200 ms post-compression, only a 40 K temperature reduction was observed near the central axis, with much of the core gas remaining homogeneous in temperature. CFD model results for laminar conditions and a compressed pressure of 39.9 bar suggest that the core gas region extends over 70% of the test chamber at 120 ms post-compression. Donovan et al.⁵² published a characterization study of a RCM with a unique sabot piston design that is capable of promoting core gas formation in a manner similar to a creviced piston. Fine-wire thermocouple measurements were recorded at multiple radial and axial locations to identify the boundaries of the adiabatic core. By defining the core region to exist anywhere that the temperature surpassed 90% of the peak-measured temperature, Donovan et al.⁵² estimated that the core region covered 50% of the test gas volume. This estimate appears to be valid up to 50 ms post-compression. It is unclear from the work by Donovan et al.⁵² how the core volume is diminished for post-compression times longer than 50 ms.

Although different RCMs typically exhibit unique heat-loss and boundary layer suppression characteristics, it should be emphasized that the piston, crevice, and bore designs used for the RCM in this work are identical to the design by Mittal and Sung.³⁰ We therefore give high regard to their previously described crevice optimization study⁴⁸ because we expect that the results may apply similarly to our RCM. Upon a more careful examination of these experimental results, it is seen that the temporal evolution of the core gas region is not clearly defined for post-compression times between 114 and 200 ms. For these two post-compression times where temperatures are measured, two considerations are noted in the broader context of this publication: (1) The homogeneity and radial extent of the core gas reported at 114 ms post-compression is adequate for testing the spray-ignition delays in the manner proposed in this paper. However, the experimental and numerical results both demonstrate that a reduction in compressed pressure leads to temperature inhomogeneities at earlier post-compression times. The extent and lifetime of the core gas region for compressed pressures of 30 bar cannot be accurately known using the results by Mittal and Sung.⁴⁸ (2) The core gas temperature inhomogeneity that appears in the measurement at 200 ms post-compression ($p_c = 39.5$ bar) is estimated to be 40 K. This magnitude of variation is unacceptable for measuring high-fidelity gas-phase ignition delay data. However, it is possible that spray-ignition delay measurements will not be significantly affected by this level of localized temperature variation. This is hypothesized because the fuel spray has significant momentum as it leaves the injector and the radial spray geometry drives a mixing process that may reduce locally confined temperature variations of this magnitude in the core region.

Given these considerations, it is prudent to investigate the effect of injection timing on the ignition delay, as an unambiguous confirmation of the test approach. To do so, five different test gas mixtures were created with varying nitrogen/argon ratios. Each mixture required a

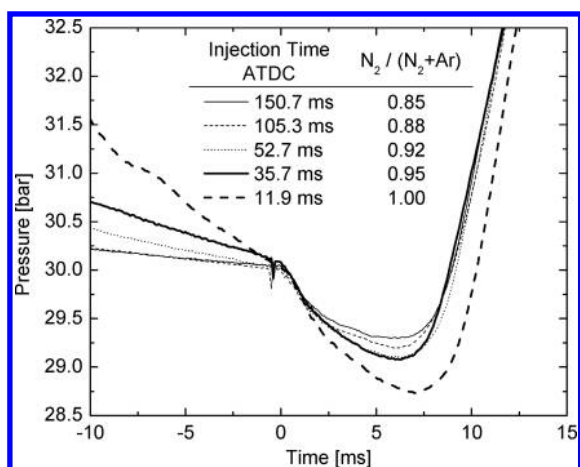


Figure 3. Pressure history data for canola BD ignition, which illustrates the independence of the ignition delay from injection timing. Injections occurred at a unique time for each test but with similar compressed temperatures (727 ± 2 K) for all tests.

unique post-compression cooling time to reach the desired compressed temperature of 727 ± 2 K. The reaction zone temperatures for these tests are 708 ± 1 K. The procedure for this calculation is presented in section 3.1. The raw pressure history data for these tests appear in Figure 3, where time $t = 0$ corresponds to the injection event. The pressure loss that occurs prior to $t = 0$ is a result of charge gas cooling, and it is clearly seen that the injection accelerates the pressure loss as energy is absorbed by the fuel spray for heating and vaporization. The timing of the ensuing pressure rise because of ignition is nearly identical for injection times of $t_{inj} \geq 35.7$ ms. For the $t_{inj} = 11.9$ ms case, the ignition appears to happen more slowly than for other cases, which is an unexpected result because the extent of the core region should be at a maximum for this test. However, it can be seen that the pre-injection pressure loss is much more rapid for this test than for the others, which can be attributed to increased gas velocities within the test chamber at such an early post-compression time. The increased charge motion enhances heat transfer to the walls, and during the ignition event, a larger amount of fuel energy must be released to overcome these losses before the pressure begins to rise.

Two ignition delay periods are used to characterize the ignition process in this study. When using the appropriate definitions in section 3.4, the first and total ignition delay periods are repeatable to within 8 and 7%, respectively, for the tests shown in Figure 3. The authors note that ignition delay measurements using a prevaporized charge in a RCM typically exhibit repeatability between 2 and 5%.^{30,53,54} These are fundamentally different types of measurements, but the comparison is indicative of the level of repeatability that is observed using more established test methods. On this basis, the proposed test approach is used to measure the ignition delays for sprays that occur up to 140 ms after the end of compression.

2.3. Injector Calibration Protocol. Before the fuel injector can be used with a fuel, it must be calibrated. A calibration curve is constructed that describes the injected mass as a function of the pulse width (i.e., injection duration). Several pulse widths are selected as calibration points, spanning the full range of injection durations that will be used in testing. For each point, three series of injections (≥ 100) are collected in a container. The total mass of the injections is determined by weighing the container before and after the test, which allows for a direct calculation of the fuel mass per injection. A linear fit is applied to the calibration data, and then it is used to determine the required pulse width for a desired injection mass. Because the pressure drop between the fuel line and the ambient environment of the injector is the primary input in

determining the injected mass, the fuel pressure is reduced to 70 bar for the calibration. This condition better matches the pressure drop between the fuel line (100 bar) and ambience during testing, where fuel is sprayed into the combustion cylinder gases at 30 bar.

3. DATA ANALYSIS

3.1. Reaction Zone Temperatures. The presentation of meaningful ignition delay and heat release rate data requires well-defined temperatures for the gas environment in which the data are measured. Calculation of the core gas temperature in a RCM is straightforward and typically proceeds through application of the adiabatic core hypothesis. As noted in section 2.2, this method assumes that the existence of a core gas region is compressed adiabatically and that actual heat losses only influence the gas temperature near the cylinder wall. In this study, a creviced piston has been used to promote the formation of an adiabatic core, which we consider valid until the injection begins. As fuel is injected into the combustion chamber, the core deteriorates and the calculated core temperature no longer adequately describes the test condition. As the liquid fuel droplets penetrate the hot gas, heat is transferred to the cool droplets for heating and vaporization. The energy required for this process reduces the temperature in the region where fuel vapor mixes with oxidizer and diluent gases. We refer to this region as the reaction zone.

Temperature calculations in the reaction zone (T_{RZ}) are based on the conservation of energy, with the adiabatic mixing assumption described by El-Wakil et al.⁵⁵ and Espey et al.⁵⁶ As thermodynamic equilibrium is established, temperatures in the reaction zone can be calculated as

$$\int_{T_{RZ}}^{T_{g,0}} C_{v,g} dT = \frac{n_f}{n_g} \left[\int_{T_{f,0}}^{T_{int}} C_{v,l} dT + h_{v,T_{int}} + \int_{T_{int}}^{T_{RZ}} C_{v,fv} dT \right] \quad (1)$$

The left-hand side of eq 1 represents the total decrease in thermal energy of the oxidizer and diluent gas mixture, which is calculated by integrating the heat capacity of the gas mixture ($C_{v,g}$) between the reaction zone temperature and the core gas temperature at the time the injection begins ($T_{g,0}$). The adiabatic core gas temperature at SOI is used as $T_{g,0}$ in eq 1. On the right-hand side, the corresponding increase in thermal energy of the fuel is represented by the term in brackets, which considers contributions from the liquid fuel heat capacity ($C_{v,l}$), the enthalpy of vaporization ($h_{v,T_{int}}$), and the fuel vapor heat capacity ($C_{v,fv}$). The liquid fuel heat capacity is integrated between the initial fuel temperature ($T_{f,0}$) and the intermediate temperature (T_{int}) at which vaporization occurs. The amount of thermal energy exchanged between the gas mixture and fuel is proportional to the ratio of fuel moles (n_f) to gas mixture moles (n_g). T_{RZ} is numerically calculated using eq 1, and for the tests presented in this study, reaction zone temperatures were 16–37 K lower than the initial core gas temperatures calculated at the SOI.

3.2. Thermophysical Properties. The reaction zone temperature and heat release rate calculations presented in the following sections rely heavily on thermophysical property data, many of which are unavailable for the methyl esters that comprise biodiesel. Similarly, diesel is a blend of numerous hydrocarbons. Its exact composition is unknown, which prevents the use of the thermodynamic property databases that provide data for individual molecules.

Biodiesel that results from the transesterification of a triglyceride with methanol is primarily comprised of five methyl

esters: methyl palmitate, methyl stearate, methyl oleate, methyl linoleate, and methyl linolenate. Because the biodiesel used in this study is canola-derived, the fraction of each of these methyl esters is estimated to be 4, 3, 60, 23, and 10%, respectively.² This composition leads to an average molecular formula estimate of $C_{18.82}H_{34.96}O_2$ for the canola BD. A limited amount of thermophysical property data is available for these biodiesel components, which includes critical temperature and enthalpy of vaporization data for the methyl esters of palmitic, stearic, and oleic acids.⁵⁷ Liquid heat capacity data are available for all of the methyl ester components; however, the experimental data is at standard temperatures, which do not match the test conditions in the RCM. When possible, these experimental data have been used to calculate reaction zone temperatures. The unavailable thermophysical property data have been estimated using group contribution methods, which assume that the properties of a substance can be estimated by summing the contributions of polyvalent atoms (i.e., groups) within the molecule.⁵⁸ The gas-phase heat capacity for all biodiesel components has been estimated using the group additivity method by Benson.⁵⁸ The method yields temperature-dependent heat capacity data for individual chemical species and is widely used in the literature for estimating heat capacity data.^{59–61} The liquid-phase heat capacities have been estimated using the method by Růžička and Domalski⁶² and the assumption that the constant-volume heat capacity and constant-pressure heat capacity are equivalent for the liquid fuels. In the original work by Růžička and Domalski,⁶² correlation predictions for esters are compared to experimental data and the predictions were within 3% of the experimental value for greater than 80% of the 85 esters tested. The enthalpies of vaporization have been estimated with the method by Tu and Liu,⁶³ which uses a three-parameter fit coupled with critical temperature data for the species of interest. Tests by Tu and Liu⁶³ indicate the method predicts the enthalpy of vaporization of esters within 5.7% of the experimental value. The group contribution method proposed by Constantinou and Gani⁶⁴ has been used to estimate critical temperatures where experimental data are not available. The method by Constantinou and Gani may be expected to predict critical temperatures within 5% of the experimental value.

For diesel fuel, where the exact composition is unknown, we have used the thermodynamic property correlations provided in the appendix by Sazhin et al.⁶⁵ The appendix provides correlations and original references for gas-phase heat capacity,⁶⁶ liquid-phase heat capacity,⁶⁶ and enthalpy of vaporization.⁶⁷ Equivalence ratios for the tests have been determined assuming an average molecular formula of $C_{14}H_{25}$.

3.3. Single-Zone Heat-Loss Model. A zero-dimensional heat-loss model was developed for the RCM to analyze the apparent heat release rates (AHRR) for biodiesel and diesel fuel in the RCM. The spray and ignition processes occurred under constant volume conditions in the RCM. Thus, by assuming ideal gas behavior, the first law of thermodynamics may be written as

$$\frac{dQ_c}{dt} = \frac{C_v V}{R_u} \frac{dp}{dt} - \frac{dQ_w}{dt} \quad (2)$$

where dQ_c/dt is the apparent rate of heat release because of combustion, C_v is the constant-volume heat capacity of the reacting gas mixture, V is the volume at the end of compression, R_u is the universal gas constant, dp/dt is the time derivative of the pressure, and dQ_w/dt is the rate of heat loss to the walls. In the first term on the right-hand side of eq 2, C_v is the only parameter

that is not determined directly from experimental data. Instead, C_v is calculated from an average cylinder temperature that is estimated using the ideal gas law and known pressure data. The second term on the right-hand side requires a heat-loss model to estimate the rate at which energy is lost through the walls of the combustion chamber. By considering convective and radiative effects, the heat loss can be estimated as

$$\frac{dQ_w}{dt} = Ah_c(T - T_w) \quad (3)$$

The constitutive equation presented in eq 3 uses Newton's law of cooling for convection losses. The convective heat losses are directly proportional to variations between the mean gas temperature (T) and wall temperature (T_w). The proportionality is dependent upon the surface area (A) of the inside of the combustion chamber and the instantaneous heat-transfer coefficient (h_c). It should be noted that the initial heat-loss model developed included a radiation heat-loss component of the form described by Annand.⁶⁸ The radiative component has been omitted from the final model because it was of negligible magnitude at our test conditions. Calculations indicated that less than 0.5% of the heat loss occurred through radiation.

Defining the instantaneous heat-transfer coefficient, h_c , in eq 3 is challenging because of the evolving conditions in the RCM during the post-compression period. This challenge is not unlike that encountered in modeling heat losses from internal combustion engines where field gradients are even more severe than experienced by the RCM charge. Many useful correlations have been proposed^{68–70} for modeling heat losses in engines, and we have chosen the well-known Hohenberg model⁷⁰ from among these as a starting point to estimate h_c . The original Hohenberg model has been applied with some success to model heat losses in homogeneous charge compression-ignition (HCCI) engines,⁷¹ and a prior study has examined the ability of the model to predict heat losses from a rapid compression expansion machine.⁷²

In the original work by Hohenberg,⁷⁰ a correlation is developed for the heat-transfer coefficient, h_c , as

$$h_c = C_1 \frac{p(\bar{v}_p + C_2)^{0.8}}{V_c^{0.06} T^{0.4}} \quad (4)$$

where p is the cylinder pressure, \bar{v}_p is the mean piston speed, V_c is the cylinder volume, and T is the mean gas temperature. Both C_1 and C_2 are arbitrary constants, for which Hohenberg proposed values of 1.30 and 1.4, respectively. The mean piston speed in eq 4 is intended to capture the influence of charge turbulence on heat loss. Although the piston in the RCM is at rest during the modeling period, charge motion will still influence heat loss. Both Mittal and Sung⁴⁸ and Würmel and Simmie⁴⁹ have published numerical studies on fluid motion in a RCM with a creviced piston. Together, these studies indicate that the peak gas velocity in the combustion chamber occurs when the piston is at TDC and quickly dissipates. Simulation results from Mittal and Sung⁴⁸ show that, for compressed pressures of 39.9 bar, using a creviced piston, the peak gas velocity decreases by 78 and 95% at 20 and 80 ms after TDC, respectively. This rapid dissipation of gas motion is markedly different from conditions in an engine and has prompted the replacement of \bar{v}_p in eq 4 with an exponentially decreasing velocity value, thus updating the original Hohenberg expression as

$$h_c = C_1 \frac{p(\bar{v}_p e^{C_2} + C_3)^{0.8}}{V_c^{0.06} T^{0.4}} \quad (5)$$

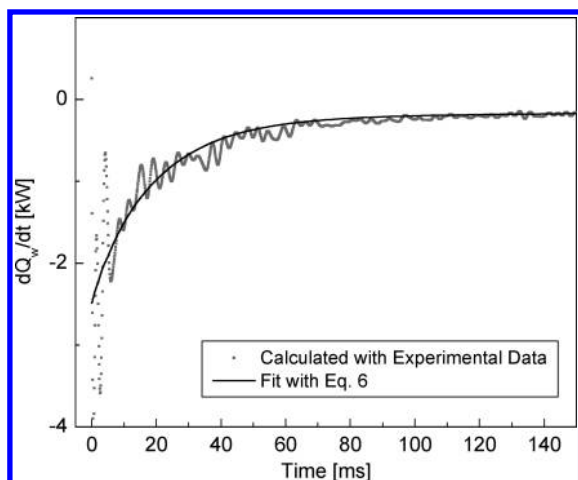


Figure 4. Sample wall heat-loss calculations from experimental data and the corresponding fit calculated using eq 6.

The mean piston speed in eq 5 is calculated using the piston speed data calculated during the compression stroke in the RCM. All other parameters are as described for eq 4. The constants C_1 , C_2 , and C_3 in eq 5 were determined using 25 non-reactive gas tests (i.e., no fuel injected) of varying compressed temperatures, compressed pressures, and mixture heat capacities. For these tests, where no combustion occurred, radiation was assumed to be negligible. Using the pressure data from the non-reactive tests, a nonlinear optimization scheme was used to determine the values of C_1 , C_2 , and C_3 , which yield the best fit for

$$\frac{C_v V}{R_u} \frac{dp}{dt} \cong AC_1 \frac{p(\bar{v}_p e^{C_2} + C_3)^{0.8}}{V_c^{0.06} T^{0.4}} (T - T_w) \quad (6)$$

For these calculations, mean gas temperatures were used and the walls were assumed to be at a constant temperature, which was equal to the initial temperature of 298 K for all tests. The analysis yielded values of $C_1 = 29.5$, $C_2 = 51.2$, and $C_3 = 0.6$. While employing these constants, we caution that Hohenberg⁷⁰ described the importance of considering combustion when calibrating the model constants. The constants that we present have been calibrated using non-reactive tests for straightforward application of eq 2, even though this may lead to some inaccuracy in the values of the optimized constants. Figure 4 compares a heat-loss profile calculated using $dQ_w/dt = (C_v V/R_u)(dp/dt)$, with the heat losses calculated using the optimized coefficients in $dQ_w/dt = AC_1(p(\bar{v}_p e^{C_2} + C_3)^{0.8})/(V_c^{0.06} T^{0.4})(T - T_w)$. It is emphasized that the model comparison and its basis are derived from heat-loss calculations using the first law of thermodynamics and not experimental measurements of the heat flux. The empirically determined fit does not reproduce the inflection point where the maximum rate of heat loss is observed shortly after TDC; however, the agreement between the two is very good for $t \geq 5$ ms after TDC, where all injections for this study have occurred. The lack of agreement during the first 5 ms after TDC is insignificant because the wall heat-loss calculations for this time period are not used in the AHRR calculations. The h_c correlation has been used to estimate wall heat losses for all ignition tests, which allows for the calculation of the AHRR using

$$\frac{dQ_c}{dt} = \frac{C_v V}{R_u} \frac{dp}{dt} - AC_1 \frac{p(\bar{v}_p e^{C_2} + C_3)^{0.8}}{V_c^{0.06} T^{0.4}} (T - T_w) \quad (7)$$

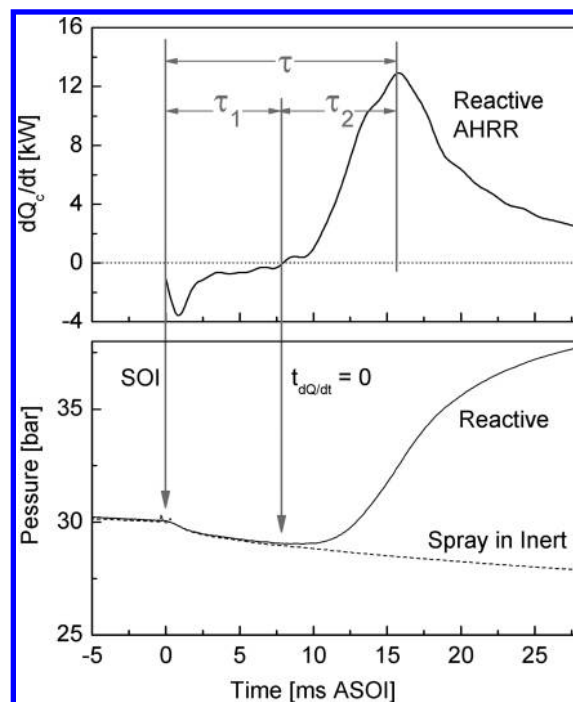


Figure 5. Definition of the ignition delay periods, τ_1 , τ_2 , and τ , using heat release rate calculations. Pressure history data for the reactive test are compared to a non-reactive test (i.e., fuel spray in an inert environment) to illustrate the pressure events occurring in corresponding time.

3.4. Ignition Delay Definition. In general, the ignition delay of a fuel is defined as the time required to autoignite after the fuel has been exposed to autoignition conditions. In our study of fuel spray ignition, we have defined two unique events during the ignition process that characterize the ignition behavior of the fuel. In the following, an approach is described that uses experimental pressure data to identify these ignition delay periods.

After fuel injection begins, the pressure in the cylinder continues to decrease because of wall heat losses and fuel evaporation. This is illustrated in Figure 5, where the pressure loss is accelerated after fuel injection at $t = 0$. Immediately following this time, the heat release rate (dQ_c/dt) calculated using the stated heat-loss model is less than zero, indicating that energy is lost not only to the walls but also to the fuel droplets. At the onset of ignition, fuel energy is released and dQ_c/dt begins to rise. The time at which dQ_c/dt becomes positive marks the first ignition delay period of interest, τ_1 , which is illustrated in Figure 5. τ_1 represents the time at which more energy is being released from fuel than is being consumed for vaporization and warming. It should be noted that τ_1 is not coincident with $dp/dt = 0$ because wall heat losses have been accounted for in the heat-loss model. This is evident in Figure 5, where the minimum pressure after injection occurs subsequent to τ_1 . The second ignition delay period of interest occurs some time, τ_2 , after τ_1 when the maximum rate of heat release because of combustion is observed. The sum total of these time periods, $\tau = \tau_1 + \tau_2$, is referred to as the total ignition delay and is illustrated in Figure 5. All ignition delays reported in this work have been calculated using these definitions. Within this definition, it is important to consider that a portion of the ignition delay time is devoted to fuel spray warming, breakup, and evaporation in the process of

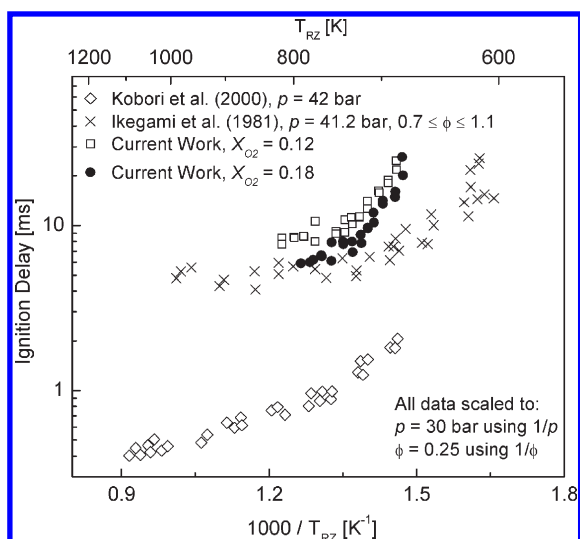


Figure 6. Comparison of measured diesel ignition delays to data published in the literature.

forming a combustible mixture. On the basis of a review of the literature,^{55,73} we would expect this to require 2–5 ms. Analysis of Figure 5 suggests it is near 2–3 ms, where the most intense heat-loss event because of the spray is seen to conclude.

3.5. Experimental Uncertainty. The preceding sections have outlined an approach for interpreting the raw pressure data recorded in the RCM. The approach is not posed as a replacement for a more rigorous treatment of the problem, which would require the application of advanced optical diagnostics and CFD model development. Such treatment is outside the scope of this study, but it is important to assess the accuracy of the analysis. In this section, we present a discussion of the uncertainty in our analysis, particularly with respect to characterizing the charge temperature and equivalence ratio.

The compressed temperature calculations that we consider valid until the SOI depend upon input data from a T-type thermocouple (Omega), an absolute pressure manometer (MKS Instruments Baratron 626B), and a piezoelectric pressure transducer (Kistler 6125B). The T-type thermocouple is used for the initial RCM temperature measurements and is specified to have an error limit of 1 °C in this temperature region. For our $p_c = 30$ bar test condition, we estimate the uncertainty in the compressed pressure to be $\pm 0.5\%$. We have used these data to estimate the maximum uncertainty in the compressed temperature calculations as ± 5 K. These compressed temperature calculations serve as the input to the reaction zone temperature calculations described by eq 1. The reaction zone temperature is seen to depend upon fuel mass injection data and thermophysical property data. Data acquired during calibration of the fuel injector indicates that the mass of fuel injected varies by $\pm 3.0\%$ ($\varphi = 0.25 \pm 0.01$). By considering the accuracy of the group contribution methods discussed in section 3.2, we estimate the maximum uncertainty in the reaction zone temperature calculations to be ± 8 K. Assigning this uncertainty still ignores the fact that we cannot expect a homogeneous temperature to exist in the core of the chamber after the fuel spray occurs; however, full multi-dimensional characterization of the temperature field is outside the scope of the applied data presented in this work. The present study requires assignment of a system reference temperature for presenting the ignition delay data, and the authors have chosen

the reaction zone temperature for this purpose. Although the reaction zone temperatures are not validated here, they are based on well-established analysis methods from the literature, and the data presented in Figure 3 support use of the reaction zone temperature as the reference temperature for studying spray ignition in the RCM.

4. RESULTS AND DISCUSSION

4.1. Comparison of Diesel Ignition Delay Measurements to the Literature Data. Figure 6 shows a comparison of the D2 ignition delay measurements recorded for this study to other measurements published in the literature. All of the published diesel ignition delays were measured using an oxygen mole fraction of $X_{O_2} = 0.21$, while the tests reported for this work used oxygen mole fractions of $X_{O_2} = 0.12$ and $X_{O_2} = 0.18$. The measurements for all of the studies were taken in a RCM, although small variations in the ignition delay definition exist between the studies. Despite this difference, a comparison among the data sets is useful to view the overall trends occurring within the data and to check for logical consistency. All of the data appearing in Figure 6 have been scaled to $p_c = 30$ bar and $\varphi = 0.25$, using the pressure scaling of $1/p$ and equivalence ratio scaling of $1/\varphi$ that are frequently referenced in the literature.^{14,17,18,74} The actual test conditions used in each of these studies appears within the legend of Figure 6.

The ignition delays recorded for this work are a full order of magnitude longer than those reported by Kobori et al.⁸ Despite the higher oxygen concentration (21%) used by Kobori et al., we do not expect this to account for all of the difference, especially considering the relatively small ignition delay reduction that is observed between the $X_{O_2} = 0.12$ and 0.18 data sets reported in this study. However, it is noted that Kobori et al. do not describe the equivalence ratio used for their testing, which may contribute to the disparity in the data. The measurements by Ikegami et al.⁹ appear to be much more consistent with the measurements reported here. The shorter ignition delays reported by Kobori et al. are likely a result of shorter evaporation and mixing times that arise because of the finer atomization that can be achieved with a high-pressure injector. The low-pressure injectors used for this study and by Ikegami et al.⁹ produce larger droplet sizes, which lead to a longer physical delay time during which evaporation and mixing occur.

Taken as a whole, the aggregate data exhibit a roll-off in the ignition delay near 800 K, where the ignition delay becomes less sensitive to changes in the temperature. This behavior suggests the presence of a negative temperature coefficient (NTC) region, where increases in the temperature lead to an increase in the chemical ignition delay time. The measurements from this study seem to be consistent with diesel ignition delays reported in the literature, and there is potential evidence of NTC behavior near the upper temperature limit that we have reported, where little change in the ignition delay is observed with changes in the reaction zone temperature. Additional measurements at higher temperatures and higher oxygen concentrations may provide a more complete comparison and additional confirmation of NTC behavior in the spray-ignition process.

4.2. Effect of the Reaction Zone Temperature on BD and D2 Ignition Delays. The ignition delay data, τ_1 and τ , measured for canola BD with $X_{O_2} = 0.12$ and 0.18 are shown in Figure 7. For the tests using $X_{O_2} = 0.12$, the first ignition delay period varied between $2.1 \leq \tau_1 \leq 10.3$ ms, while the total ignition delay varied

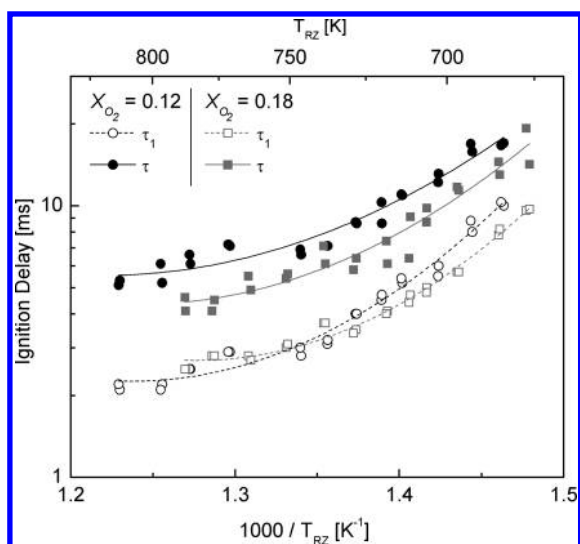


Figure 7. Ignition delay measurements (τ_1 and τ) for canola BD sprays in oxidizing environments with $X_{O_2} = 0.12$ and 0.18 .

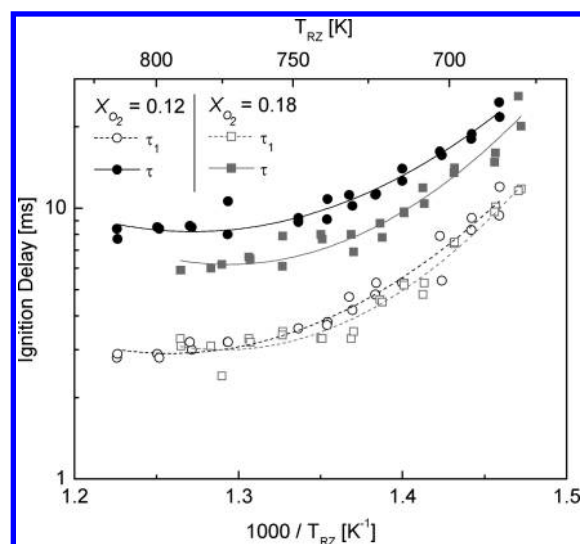


Figure 8. Ignition delay measurements (τ_1 and τ) for D2 sprays in oxidizing environments with $X_{O_2} = 0.12$ and 0.18 .

between $5.1 \leq \tau \leq 17.0$ ms. For the tests using $X_{O_2} = 0.18$, the first ignition delay period varied between $2.5 \leq \tau_1 \leq 9.7$ ms, while the total ignition delay varied between $4.1 \leq \tau \leq 19.3$ ms. There is evidence of potential NTC behavior near the upper limit of the reaction zone temperatures that were tested. This can be observed near $T_{RZ} = 770$ K, where both the τ_1 and τ data become less sensitive to increases in the temperature. The evidence of NTC behavior in a spray-ignition measurement was not fully anticipated because the physical and chemical ignition delays are tightly convolved. For some test conditions, it may be expected that small changes in the chemical ignition delay would be overwhelmed by the physical effects. The diesel spray-ignition study by Kobori et al.⁸ did report NTC behavior for some of the spray-ignition measurements but only for injector orifice sizes between 25 and 100 μm . The orifice size of the injector used for this study approaches 200 μm , and Kobori et al.⁸ did not observe NTC behavior when testing with a similar orifice size. Another important observation from Figure 7 is that the fuel and oxygen concentrations have an obvious influence on the total ignition delay period. However, the τ_1 data for both oxygen concentrations are remarkably similar, and the two data sets are not easily distinguished from one another over the tested temperature domain. We do, however, see separation in the two data sets near the lower limit of tested temperatures. We interpret this finding to mean that fuel kinetics play an increasingly important role at lower temperatures but that, at higher temperatures, the first ignition delay period may be dominated by physical transport processes, such as spray breakup and evaporation. Near $T_{RZ} = 750$ K, we observe a crossover in the two τ_1 data sets. Within the precision of the data, we cannot say this occurrence has significance but it does motivate future studies at higher temperatures and additional oxygen mole fractions. The increased availability of oxygen, however, does subsequently lead to more rapid fuel oxidation and a reduction in the time required to reach the maximum rate of heat release. As previously described, the tests were carried out for the constant bulk equivalence ratio of $\phi = 0.25$; thus, the injections for the $X_{O_2} = 0.18$ tests carry 50% more mass than the $X_{O_2} = 0.12$ tests. The increased fuel mass leads to additional radicals that

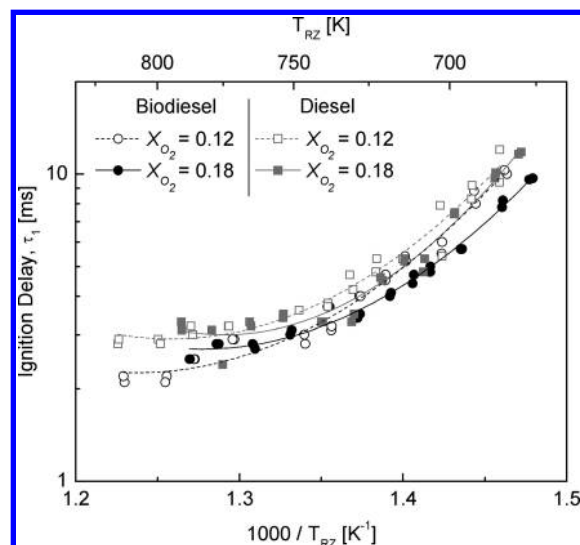


Figure 9. Comparison of ignition delay period τ_1 for canola BD and D2 fuel sprays in oxidizing environments with $X_{O_2} = 0.12$ and 0.18 .

contribute to the low-temperature chain-branching mechanism and, hence, faster ignition.

A similar set of ignition delay data for D2 are presented in Figure 8, where τ_1 and τ measurements are presented for spray-ignition tests in oxidizing environments with $X_{O_2} = 0.12$ and 0.18 . For the tests using $X_{O_2} = 0.12$, the first ignition delay period varied between $2.8 \leq \tau_1 \leq 12.0$ ms, while the total ignition delay varied between $7.7 \leq \tau \leq 24.6$ ms. For the tests using $X_{O_2} = 0.18$, the first ignition delay period varied between $2.4 \leq \tau_1 \leq 11.8$ ms, while the total ignition delay varied between $5.9 \leq \tau \leq 25.9$ ms. The overall trends are quite similar to those observed for the BD ignition delays, with evidence of NTC behavior becoming visible near $T_{RZ} = 740$ K, where the ignition delays become less sensitive to increases in the temperature. This corresponds very well with the published data by Kobori et al.,⁸ which indicates the onset of NTC behavior in diesel spray ignition between 730 and 745 K.

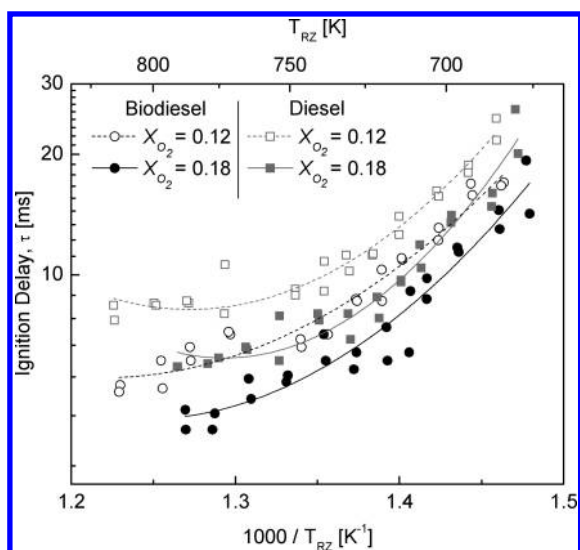


Figure 10. Comparison of ignition delay period τ for canola BD and D2 fuel sprays in oxidizing environments with $X_{O_2} = 0.12$ and 0.18 .

As with the BD results, the τ_1 measurements for D2 sprays show little sensitivity to the oxygen and fuel concentration change, while a marked reduction in τ is observed as the oxygen mole fraction increases from $X_{O_2} = 0.12$ to 0.18 . The increase in the oxygen mole fraction also leads to increased fuel mass concentration because all tests use $\phi = 0.25$. As with our discussion of the τ_1 data for the canola BD tests, we would expect fuel kinetics to play an increasingly important role for longer delays. For τ_1 measurements longer than 3 ms, data from the $X_{O_2} = 0.12$ data set appear to be longer than for the $X_{O_2} = 0.18$ data, but we are cautious to draw this conclusion given the precision of the data.

The data from Figures 7 and 8 are plotted again in Figures 9 and 10 to allow for a direct comparison of the BD and D2 ignition delays using the same carbon concentrations for each fuel. Figure 9 shows that, although the first ignition delay period for BD is shorter than for D2 over the range of tested reaction zone temperatures, the difference between the two fuels is quite small. In fact, over the full range of tested reaction zone temperatures, nonlinear least-squares fits were used to calculate that, on average, the τ_1 ignition delay measurements for BD are only 0.6 ms (−12%) and 0.8 ms (−16%) shorter at $X_{O_2} = 0.12$ and 0.18 , respectively. Given the uncertainty of the measurements, these are effectively the same. We do note that a longer physical delay is expected for BD relative to D2 based on the physical properties of the two fuels (i.e., higher viscosity and surface tension for BD relative to D2). If the τ_1 measurements are in fact shorter for BD than D2, we expect this indicates that kinetics plays an important role in determining τ_1 . For the τ measurements, the disparity between the two fuels grows and the BD measurements are shorter than the D2 measurements by 3.0 ms (−23%) and 2.3 ms (−23%) at $X_{O_2} = 0.12$ and 0.18 , respectively. A longer total ignition delay period for D2 is consistent with our expectations based on the reported cetane number for the fuels. A typical D2 cetane number is 47,³⁸ while canola BD cetane numbers have been reported between 47.9 and 56.^{32,75,76} The direct comparison of the two fuels also illustrates that evidence of potential NTC behavior occurs for the D2 spray-ignition measurements at lower reaction zone temperatures than for the canola BD. Furthermore, the data suggest that the NTC region may be

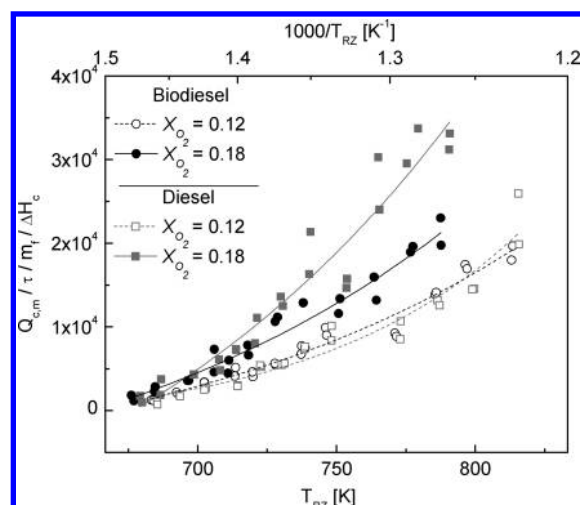


Figure 11. Comparison of maximum AHRR data normalized by total ignition delay time for canola BD and D2 fuel sprays in oxidizing environments with $X_{O_2} = 0.12$ and 0.18 .

more pronounced for D2 than for canola BD. The kinetics that would lead to NTC behavior are known to strongly depend upon the competition between decomposition reactions of the alkyl hydroperoxy radical and the oxygen addition reaction that leads to low-temperature chain-branching reactions.⁷⁷ The competition between these reaction pathways depends upon the fuel structure, such as molecular unsaturation and branching in the alkyl chain. For example, unsaturation in ester compounds, such as the biodiesel components, is known to decrease low-temperature reactivity.⁷⁸ We expect these influences to affect the observed onset of NTC-like behavior, but among the complicated blend of fuel species and transport processes, we present these only as considerations when interpreting the data.

4.3. Effect of the Reaction Zone Temperature on the Maximum Normalized AHRR of BD and D2. The maximum normalized AHRR $1/(\tau m_f \Delta H_c) \dot{Q}_{c,m} = \dot{Q}_{c,m}$ calculations for BD and D2 test cases appear in Figure 11 for both $X_{O_2} = 0.12$ and 0.18 . These data points have been calculated by taking the maximum observed AHRR value for a given test and dividing it by the total ignition delay time measurement and the input energy for that test. The input energy is calculated by multiplying the mass of the fuel injection by the lower heating value (ΔH_c) of the fuel. We have chosen to normalize these data because, at a given temperature, the ignition delays for the BD and D2 test fuels are different, which will lead to a variation in the size of the premixed volume. A longer ignition delay will provide additional time for premixture formation and augment the maximum observed AHRR. Similarly, the injected fuel energy will strongly influence the peak heat release rate for a test and should be accounted for when analyzing the data. The normalization isolates the influence of the temperature on the maximum AHRR from the effects of input fuel energy and the premixing time.

For the $X_{O_2} = 0.12$ tests, the $\dot{Q}_{c,m}$ data for BD and D2 data are very similar at all reaction zone temperatures. This result suggests that the rate of reaction for the $X_{O_2} = 0.12$ tests is limited by the low oxygen concentrations in the reaction zone. A diesel fuel blend contains some components that are more volatile than the methyl esters that comprise biodiesel. At a given temperature, these D2 fuel components are more readily volatilized, which should lead to a larger premixed volume relative to the BD tests.

On the basis of this description, we would expect the $\dot{Q}_{c,m}$ values for D2 to be larger than for BD; however, this is not the case for these low oxygen concentrations. We suspect that this occurs because there is insufficient oxygen to react with all of the fuel in the reaction zone. Although the D2 fuel volatilizes more quickly than BD and, thus, begins mixing with oxidizer gases at an earlier stage, a portion of this fuel remains unreacted and does not appear to contribute to increasing $\dot{Q}_{c,m}$. A comparison of the $\dot{Q}_{c,m}$ data for the $X_{O_2} = 0.18$ tests in Figure 11 clearly demonstrates that D2 exhibits greater maximum normalized AHRR than BD at increased temperatures. The $\dot{Q}_{c,m}$ data for D2 and BD are similar for reaction zone temperatures near 700 K but diverge for temperature increases beyond this point, with the maximum normalized AHRR of both fuels demonstrating an exponential dependence upon the reaction zone temperature. The application of our hypothesis regarding the $X_{O_2} = 0.12$ results to these data implies that the increased oxygen concentration in the $X_{O_2} = 0.18$ tests provides sufficient oxygen to react with more of the volatilized D2 fuel than the tests using $X_{O_2} = 0.12$. On the basis of this hypothesis, we may expect an additional gain in $\dot{Q}_{c,m}$ by further increasing the oxygen concentration.

5. CONCLUSION

A rapid compression machine has been used to investigate the autoignition delay times and maximum AHRR of canola BD and D2 sprays under test conditions that are relevant to the LTC regime in diesel engine combustion. The ignition delay and AHRR measurements have been taken at various oxygen mole fractions ($X_{O_2} = 0.12$ and 0.18) and various reaction zone temperatures ($676 \leq T_{RZ} \leq 816$ K), which were investigated by altering the diluent composition and the post-compression cooling time. The viability of this test approach has been examined, and tests show that, for post-compression cooling times between 11.9 and 150.8 ms, the first and total ignition delay periods are repeatable to within 8 and 7%, respectively.

Test temperatures in the reaction zone have been numerically calculated using the adiabatic mixing assumption proposed by El-Wakil et al.⁵⁵ This approach accounts for temperature reductions in the reaction zone, which occur as energy is transferred from the hot gas to the cooler fuel droplets for warming and vaporization. A single-zone heat-loss model has been developed that calculates convective heat losses using a modification to the approach described by Hohenberg.⁷⁰ The calculated heat-loss profiles have been used as a basis for calculating two ignition delay periods.

The total ignition delay measurements for D2 are compared to values reported in the literature. The measurements that we report are not at identical test conditions to those in the literature, but when scaled, our data exhibit logical consistency with the literature data. A comparison to other diesel spray-ignition studies indicates that the orifice size of the injector and the injection pressure may strongly influence the total ignition delay of D2. The ignition delay data for D2 and BD exhibit potential evidence of NTC behavior near the upper limit of the tested temperatures for both oxygen mole fractions tested. This is observed through decreased ignition delay sensitivity to changes in the temperature. The reduction in temperature sensitivity occurs near $T_{RZ} = 740$ K for the D2 measurements, which is consistent with literature data. For BD, the decreased temperature sensitivity becomes evident at a higher reaction zone temperature of $T_{RZ} = 770$ K. At similar test conditions, the total

ignition delay period of BD was on average 23% shorter than for D2 at oxygen mole fractions of $X_{O_2} = 0.12$ and 0.18 . Although the first ignition delay period was shorter for BD than for D2, the average results differed by less than 1 ms. Increases in the oxygen mole fraction at a given reaction zone temperature led to a reduction in the total ignition delay for both BD and D2 but had little to no influence on the first ignition delay period.

The maximum normalized AHRR data for the BD and D2 fuels were compared over the full range of reaction zone temperatures, with the data exhibiting an exponential dependence upon the reaction zone temperature at both oxygen fractions (12 and 18%). The results appear to be largely influenced by the amount of oxygen available in the reaction zone to react with volatilized fuel. We expect the increased volatility of D2 to enhance the extent of the premixture relative to BD and, thus, lead to larger maximum normalized AHRR values. However, this is only conclusively observed for the $X_{O_2} = 0.18$ tests, where sufficient oxygen exists to react with more of the volatilized D2 fuel.

Increases in the reaction zone temperature led to modest increases in maximum AHRR for BD, but a more pronounced increase in the AHRR was observed for D2 over the same set of reaction zone temperatures. We hypothesize that the greater temperature sensitivity of the D2 maximum AHRR occurs because the more volatile components of D2 readily enter the vapor phase at higher temperatures and increase the extent of the premixture prior to ignition. The maximum AHRR is augmented for both BD and D2 as the oxygen mole fraction increases; however, the D2 maximum AHRR is greatly enhanced for the $X_{O_2} = 0.18$ tests at higher temperatures, where the volatilized D2 components burn more rapidly with the more plentiful oxygen.

The results presented here form a basis for comparing the spray-ignition properties of two fuels under practical engine conditions, where the chemical ignition process is tightly coupled to the physical transport processes, such as spray breakup and evaporation. The data demonstrate the ability to differentiate between the spray-ignition properties of different fuels and to potentially identify subtle ignition features, such as NTC behavior. Future studies will be devoted to investigate the spray-ignition characteristics of fuels with changes in the molecular structure, to identify molecular features, which lead to significant changes in the total physical and chemical ignition delays of a fuel.

■ AUTHOR INFORMATION

Corresponding Author

*Telephone: (517) 432-3187. E-mail: tonghun@msu.edu.

■ ACKNOWLEDGMENT

The authors gratefully acknowledge the financial support of the U.S. Department of Energy (Contract DE-FC26-07NT43278) in the completion of this work.

■ REFERENCES

- (1) Demirbas, A. Biofuels securing the planet's future energy needs. *Energy Convers. Manage.* **2009**, *50* (9), 2239.
- (2) Knothe, G.; Krahl, J.; Gerpen, J. V. *The Biodiesel Handbook*; American Oil Chemists' Society (AOCS) Press: Champaign, IL, 2005.
- (3) Lapuerta, M.; Armas, O.; Rodríguez-Fernández, J. Effect of biodiesel fuels on diesel engine emissions. *Prog. Energy Combust. Sci.* **2008**, *34* (2), 198.

- (4) Lefebvre, A. H.; Mellor, A. M.; Peters, J. E. *Ignition/Stabilization/Atomization—Alternative Fuels in Gas Turbine Combustors*; Bowman, C. T., Birkeland, J., Eds.; American Institute of Aeronautics and Astronautics (AIAA): Reston, VA, 1978; Vol. 62, pp 137–159.
- (5) Peters, J. E.; Mellor, A. M. An ignition model for quiescent fuel sprays. *Combust. Flame* **1980**, *38*, 65–74.
- (6) Azimov, U.; Kim, K.; Jeong, D.; Lee, Y. Evaluation of low-temperature diesel combustion regimes with *n*-heptane fuel in a constant-volume chamber. *Int. J. Automot. Technol.* **2009**, *10* (3), 265–276.
- (7) Dec, J. E. Advanced compression-ignition engines—Understanding the in-cylinder processes. *Proc. Combust. Inst.* **2009**, *32* (2), 2727.
- (8) Kobori, S.; Kamimoto, T.; Aradi, A. A study of ignition delay of diesel fuel sprays. *Int. J. Engine Res.* **2000**, *1* (1), 29–39.
- (9) Ikegami, M.; Miwa, K.; Inada, M. A study on ignition and combustion of a diesel spray by means of a rapid compression machine. *Bull. JSME* **1981**, *24* (195), 1608–1615.
- (10) Miwa, K.; Ohmiya, T.; Nishiwaki, T. A study of the ignition delay of diesel fuel spray using a rapid compression machine. *JSME Int. J., Ser. II* **1988**, *31* (1), 166.
- (11) Edwards, C. F.; Siebers, L. D. A study of the autoignition process of a diesel spray via high speed visualization. *SAE [Tech. Pap.]* **1992**No. 920108.
- (12) Callahan, T. J.; Ryan, T. W. Engine and constant volume bomb studies of diesel ignition and combustion. *SAE [Tech. Pap.]* **1988**No. 881626.
- (13) Wolfer, H. H. Der zundverzug im dieselmotor. *VDI-Forschungsh.* **1938**, *392*, 15.
- (14) Assanis, D. N.; Filipi, Z. S.; Fiveland, S. B.; Syrimis, M. A predictive ignition delay correlation under steady-state and transient operation of a direct injection diesel engine. *J. Eng. Gas Turbines Power* **2003**, *125* (2), 450–457.
- (15) Callahan, C. V.; Held, T. J.; Dryer, F. L.; Minetti, R.; Ribaucour, M.; Sochet, L. R.; Faravelli, T.; Gaffuri, P.; Rani, E. Experimental data and kinetic modeling of primary reference fuel mixtures. *Symp. (Int.) Combust., [Proc.]* **1996**, *26* (1), 739.
- (16) Hardenberg, H. O.; Hase, F. W. An empirical formula for computing the pressure rise delay of a fuel from its cetane number and from the relevant parameters of direct-injection diesel engines. *SAE Trans.* **1979**, *88*, No. 790493.
- (17) Spadaccini, L. J.; Tevelde, J. A. Autoignition characteristics of aircraft-type fuels. *Combust. Flame* **1982**, *46*, 283–300.
- (18) Haylett, D. R.; Lappas, P. P.; Davidson, D. F.; Hanson, R. K. Application of an aerosol shock tube to the measurement of diesel ignition delay times. *Proc. Combust. Inst.* **2008**, *32*, 477–484.
- (19) Dagaut, P.; Gail, S.; Sahasrabudhe, M. Rapeseed oil methyl ester oxidation over extended ranges of pressure, temperature, and equivalence ratio: Experimental and modeling kinetic study. *Proc. Combust. Inst.* **2007**, *31* (2), 2955–2961.
- (20) Hakka, M. H.; Glaude, P.-A.; Herbinet, O.; Battin-Leclerc, F. Experimental study of the oxidation of large surrogates for diesel and biodiesel fuels. *Combust. Flame* **2009**, *156* (11), 2129–2144.
- (21) Bax, S.; Hakka, M. H.; Glaude, P.-A.; Herbinet, O.; Battin-Leclerc, F. Experimental study of the oxidation of methyl oleate in a jet-stirred reactor. *Combust. Flame* **2010**, *157* (6), 1220–1229.
- (22) Schönborn, A.; Ladommatos, N.; Williams, J.; Allan, R.; Rogerson, J. Effects on diesel combustion of the molecular structure of potential synthetic bio-fuel molecules. *SAE [Tech. Pap.]* **2007**No. 2007-24-0125.
- (23) Schönborn, A.; Ladommatos, N.; Williams, J.; Allan, R.; Rogerson, J. The influence of molecular structure of fatty acid monoalkyl esters on diesel combustion. *Combust. Flame* **2009**, *156* (7), 1396.
- (24) Pastor, J. V.; Payri, R.; Gimeno, J.; Nerva, J. G. Experimental study on RME blends: Liquid-phase fuel penetration, chemiluminescence, and soot luminosity in diesel-like conditions. *Energy Fuels* **2010**, *25* (2), 843–843.
- (25) Vaughn, T.; Hammill, M.; Harris, M.; Marchese, A. Ignition delay of bio-ester fuel droplets. *Proceedings of the Society of Automotive Engineers (SAE) Powertrain and Fluid Systems Conference and Exhibition*; Toronto, Canada, Oct 16–19, 2006; SAE Paper 2006-01-3302.
- (26) Marchese, A. J.; Vaughn, T. L.; Kroenlein, K.; Dryer, F. L. Ignition delay of fatty acid methyl ester fuel droplets: Microgravity experiments and detailed numerical modeling. *Proc. Combust. Inst.* **2011**, *33* (2), 2021–2030.
- (27) Knothe, G.; Matheaus, A. C.; Ryan, T. W. Cetane numbers of branched and straight-chain fatty esters determined in an ignition quality tester. *Fuel* **2003**, *82* (8), 971–975.
- (28) Knothe, G. Dependence of biodiesel fuel properties on the structure of fatty acid alkyl esters. *Fuel Process. Technol.* **2005**, *86* (10), 1059–1070.
- (29) Knothe, G. “Designer” biodiesel: Optimizing fatty ester composition to improve fuel properties. *Energy Fuels* **2008**, *22* (2), 1358–1364.
- (30) Mittal, G.; Sung, C. J. A rapid compression machine for chemical kinetics studies at elevated pressures and temperatures. *Combust. Sci. Technol.* **2007**, *179*, 497–530.
- (31) Allen, C.; Mittal, G.; Sung, C.-J.; Toulson, E.; Lee, T. An aerosol rapid compression machine for studying energetic-nanoparticle-enhanced combustion of liquid fuels. *Proc. Combust. Inst.* **2011**, *33* (2), 3367–3374.
- (32) Bouché, T.; Hinz, M.; Pittermann, R.; Herrmann, M. Optimising tractor CI engines for biodiesel operation. *SAE [Tech. Pap.]* **2000** No. 2000-01-1969.
- (33) Alptekin, E.; Canakci, M. Determination of the density and the viscosities of biodiesel–diesel fuel blends. *Renewable Energy* **2008**, *33* (12), 2623–2630.
- (34) Allen, C.; Watts, K.; Ackman, R. Predicting the surface tension of biodiesel fuels from their fatty acid composition. *J. Am. Oil Chem. Soc.* **1999**, *76* (3), 317–323.
- (35) Ejim, C. E.; Fleck, B. A.; Amirfazli, A. Analytical study for atomization of biodiesels and their blends in a typical injector: Surface tension and viscosity effects. *Fuel* **2007**, *86* (10–11), 1534–1544.
- (36) Yuan, W.; Hansen, A. C.; Zhang, Q. Vapor pressure and normal boiling point predictions for pure methyl esters and biodiesel fuels. *Fuel* **2005**, *84* (7–8), 943.
- (37) *MSDS Summary Sheet: No. 2 Diesel Fuel*; Phillips Petroleum Company: Bartlesville, OK, 2002.
- (38) Goering, C. E.; Schwab, A. W.; Daugherty, M. J.; Pryde, E. H.; Heakin, A. J. Fuel properties of eleven vegetable oils. *Trans. ASAE* **1982**, *25* (6), 1472–1477.
- (39) Canakci, M.; Van Gerpen, J. H. Comparison of engine performance and emissions for petroleum diesel fuel, yellow grease biodiesel, and soybean oil biodiesel. *Trans. ASABE* **2003**, *46* (4), 937–944.
- (40) Tsolakis, A.; Golunski, S. E. Sensitivity of process efficiency to reaction routes in exhaust-gas reforming of diesel fuel. *Chem. Eng. J.* **2006**, *117* (2), 131–136.
- (41) Tanaka, S.; Ayala, F.; Keck, J. C. A reduced chemical kinetic model for HCCI combustion of primary reference fuels in a rapid compression machine. *Combust. Flame* **2003**, *133* (4), 467–481.
- (42) Jung, D.; Assanis, D. N. Multi-zone DI diesel spray combustion model for cycle simulation studies of engine performance and emissions. *SAE [Tech. Pap.]* **2001**No. 2001-01-1246.
- (43) Park, P. *Rapid Compression Machine Measurements of Ignition Delays for Primary Reference Fuels*; Massachusetts Institute of Technology (MIT): Cambridge, MA, 1990.
- (44) Lee, D.; Hochgreb, S. Rapid compression machines: Heat transfer and suppression of corner vortex. *Combust. Flame* **1998**, *114* (3), 531–545.
- (45) Clarkson, J.; Griffiths, J. F.; MacNamara, J. P.; Whitaker, B. J. Temperature fields during the development of combustion in a rapid compression machine. *Combust. Flame* **2001**, *125* (3), 1162.
- (46) Griffiths, J. F.; Jiao, Q.; Kordylewski, W.; Schreiber, M.; Meyer, J.; Knoche, K. F. Experimental and numerical studies of ditertiary butyl peroxide combustion at high pressures in a rapid compression machine. *Combust. Flame* **1993**, *93* (3), 303–315.
- (47) Desgroux, P.; Gasnot, L.; Sochet, L. R. Instantaneous temperature measurement in a rapid-compression machine using laser Rayleigh scattering. *Appl. Phys. B: Lasers Opt.* **1995**, *61* (1), 69–72.
- (48) Mittal, G.; Sung, C.-J. Aerodynamics inside a rapid compression machine. *Combust. Flame* **2006**, *145* (1–2), 160.

- (49) Würmel, J.; Simmie, J. M. CFD studies of a twin-piston rapid compression machine. *Combust. Flame* **2005**, *141* (4), 417.
- (50) Donovan, M. T.; He, X.; Palmer, T. R.; Zigler, B. T.; Wooldridge, M. S. Demonstration of a free-piston rapid compression facility for the study of high temperature combustion phenomenon. *Combust. Flame* **2004**, *137*, 351–365.
- (51) Park, P.; Keck, J. C. Rapid compression machine measurements of ignition delays for primary reference fuels. *SAE Trans.* **1990**, *99* (900027), 11–23.
- (52) Donovan, M. T.; He, X.; Zigler, B. T.; Palmer, T. R.; Wooldridge, M. S.; Atreya, A. Demonstration of a free-piston rapid compression facility for the study of high temperature combustion phenomena. *Combust. Flame* **2004**, *137* (3), 351–365.
- (53) Tanaka, S.; Ayala, F.; Keck, J. C.; Heywood, J. B. Two-stage ignition in HCCI combustion and HCCI control by fuels and additives. *Combust. Flame* **2003**, *132* (1–2), 219.
- (54) Gersen, S.; Mokhov, A. V.; Darneveil, J. H.; Levinsky, H. B. Ignition properties of *n*-butane and iso-butane in a rapid compression machine. *Combust. Flame* **2010**, *157* (2), 240–245.
- (55) El-Wakil, M. M.; Myers, P. S.; Uyehara, O. A. Fuel vaporization and ignition lag in diesel combustion. *SAE Trans.* **1956**, *64*, 712–726.
- (56) Espey, C.; Dec, J. E.; Litzinger, T. A.; Santavicca, D. A. Planar laser Rayleigh scattering for quantitative vapor-fuel imaging in a diesel jet. *Combust. Flame* **1997**, *109* (1–2), 65–78.
- (57) Yaws, C. L. *Yaws' Thermophysical Properties of Chemicals and Hydrocarbons*; Knovel: Norwich, NY, 2009.
- (58) Benson, S. W. *Thermochemical Kinetics*; John Wiley and Sons, Inc.: New York, 1968; p 223.
- (59) Herbinet, O.; Pitz, W. J.; Westbrook, C. K. Detailed chemical kinetic oxidation mechanism for a biodiesel surrogate. *Combust. Flame* **2008**, *154* (3), 507–528.
- (60) Ritter, E. R. THERM: A computer code for estimating thermodynamic properties for species important to combustion and reaction modeling. *J. Chem. Inf. Comput. Sci.* **1991**, *31* (3), 400–408.
- (61) Ritter, E. R.; Bozzelli, J. W. THERM: Thermodynamic property estimation for gas phase radicals and molecules. *Int. J. Chem. Kinet.* **1991**, *23* (9), 767–778.
- (62) Růžička, V., Jr.; Domalski, E. S. Estimation of the heat capacities of organic liquids as a function of temperature using group additivity. II. Compounds of carbon, hydrogen, halogens, nitrogen, oxygen, and sulfur. *J. Phys. Chem. Ref. Data* **1993**, *22* (3), 619–657.
- (63) Tu, C.-H.; Liu, C.-P. Group-contribution estimation of the enthalpy of vaporization of organic compounds. *Fluid Phase Equilib.* **1996**, *121* (1–2), 45–65.
- (64) Constantinou, L.; Gani, R. New group contribution method for estimating properties of pure compounds. *AIChE J.* **1994**, *40* (10), 1697–1710.
- (65) Sazhin, S. S. Advanced models of fuel droplet heating and evaporation. *Prog. Energy Combust. Sci.* **2006**, *32* (2), 162–214.
- (66) Durrett, R. P.; Oren, D. C.; Ferguson, C. R. A multidimensional data set for diesel combustion model validation: I. Initial conditions, pressure history and spray shapes. *SAE [Tech. Pap.]* **1987**No. 872087.
- (67) Chin, J. S.; Lefebvre, A. H. The role of the heat-up period in fuel drop evaporation. *Int. J. Turbo Jet Engines* **1985**, *2*, 315–325.
- (68) Annand, W. J. D. Heat transfer in the cylinders of reciprocating internal combustion engines. *Proc. Inst. Mech. Eng.* **1963**, *177*, 973–990.
- (69) Woschni, G. A universally applicable equation for the instantaneous heat transfer coefficient in the internal combustion engine. *SAE [Tech. Pap.]* **1967**No. 670931.
- (70) Hohenberg, G. F. Advanced approaches for heat transfer calculations. *SAE [Tech. Pap.]* **1979**No. 790825.
- (71) Soyhan, H. S.; Yasar, H.; Walmsley, H.; Head, B.; Kalghatgi, G. T.; Sorusbay, C. Evaluation of heat transfer correlations for HCCI engine modeling. *Appl. Therm. Eng.* **2009**, *29* (2–3), 541–549.
- (72) Goldsborough, S. S. Evaluating the heat losses from HCCI combustion within a rapid compression expansion machine. *SAE [Tech. Pap.]* **2006**No. 2006-01-0870.
- (73) Wolff, M. C.; Meisl, J.; Koch, R.; Wittig, S. The influence of evaporation on the autoignition-delay of *n*-heptane air mixtures under gas turbine conditions. *Symp. (Int.) Combust., [Proc.]* **1998**, *27* (2), 2025–2031.
- (74) Watson, N.; Pilley, A. D.; Marzouk, M. A combustion correlation for diesel engine simulation. *SAE [Tech. Pap.]* **1980**No. 800029.
- (75) Avella, F.; Galtieri, A.; Fiumara, A. Characteristics and utilization of vegetable derivatives as diesel fuels. *Riv. Combust.* **1992**, *46* (6), 181–188.
- (76) Krahl, J.; Baum, K.; Hackbarth, U.; Jeberien, H. E.; Schröder, A. M. C. S. O.; Walter, N.; Bünger, J.; Müller, M. M.; Weigel, A. Gaseous compounds, ozone precursors, particle number and particle size distributions, and mutagenic effects due to biodiesel. *Trans. ASAE* **2001**, *44* (2), 179–191.
- (77) Westbrook, C. K. Chemical kinetics of hydrocarbon ignition in practical combustion systems. *Proc. Combust. Inst.* **2000**, *28* (2), 1563.
- (78) Zhang, Y.; Yang, Y.; Boehman, A. L. Premixed ignition behavior of C9 fatty acid esters: A motored engine study. *Combust. Flame* **2009**, *156* (6), 1202–1213.